J. Fluid Mech. (2007), *vol.* 576, *pp.* 457–473.
doi:10.1017/S0022112006004526 Printed in the United Kingdom

Scaling of the wall-normal turbulence component in high-Reynolds-number pipe flow

RONGRONG ZHAO† AND ALEXANDER J. SMITS

Department of Mechanical and Aerospace Engineering, Princeton University, Princeton, NJ 08544, USA

(Received 22 June 2006 and in revised form 1 November 2006)

Streamwise and wall-normal turbulence components are obtained in fully developed turbulent pipe over a Reynolds number range from 1.1×10^5 to 9.8×10^6. The streamwise intensity data are consistent with previous measurements in the same facility. For the wall-normal turbulence intensity, a constant region in $v'_{\mathrm{r.m.s.}}$ is found for the region $200 \leqslant y^+ \leqslant 0.1R^+$ for Reynolds numbers up to 1.0×10^6. An increase in $v'_{\mathrm{r.m.s.}}$ is observed below about $y^+ \sim 100$, although additional measurements will be required to establish its generality. The wall-normal spectra collapse in the energy-containing region with inner scaling, but for the low-wavenumber region a y/R dependence is observed, which also indicates a continuing influence from the outer flow on the near-wall motions.

1. Introduction

High-Reynolds-number wall-bounded flows are of interest because they encompass many industrial and geophysical applications. To learn more about these flows, and in particular, to explore their Reynolds number scaling, a number of recent studies have been performed. Boundary layer investigations by Fernholz *et al.* (1995), Hites (1997), Österlund (1999), and DeGraaff & Eaton (2000) cover Reynolds numbers up to about $Re_\theta = 6.2 \times 10^4$, where $Re_\theta = U_e\theta/\nu$, U_e is the free-stream velocity, θ the momentum thickness, and ν the kinematic viscosity. Although these Reynolds numbers may seem large, McKeon & Morrison (2005) have suggested they are not large enough to reveal the asymptotic high-Reynolds-number behaviour. Studies of neutrally buoyant atmospheric surface layers offer much higher Reynolds numbers, closer to about $Re_\theta = 10^6$ (Metzger *et al.* 2001; Nickels *et al.* 2005; Kunkel & Marusic 2006), but there are well-documented difficulties in acquiring accurate and detailed turbulence measurements in such flows. In this respect, pipe flows are very useful, and recent work by Zagarola & Smits (1998), McKeon *et al.* (2004) and Morrison *et al.* (2004) have yielded mean flow data for $3.1 \times 10^4 \leqslant Re_D \leqslant 3.5 \times 10^7$, and measurements of the streamwise component of turbulence for $5.5 \times 10^4 \leqslant Re_D \leqslant 5.7 \times 10^6$. Here, Re_D is the Reynolds number based on the pipe diameter D and the bulk velocity $\overline{U}$. For the purpose of comparing boundary layer and pipe flows, the equivalence between Reynolds numbers may be taken as $Re_D \approx 20Re_\theta$ (assuming $\theta/\delta \approx 0.1$, and $\delta = O(R)$, where R is the pipe radius and δ is the boundary layer thickness). Therefore the highest boundary layer Reynolds number found in the laboratory is equivalent to a pipe flow of only about 10^6, and therefore pipe flows are well suited for studies of very

† Present address: Geophysical Fluid Dynamics Laboratory, Princeton, NJ, USA.

Experiments	Reynolds number	Component
Laufer (1954)	$5.0 \times 10^4 \sim 5.0 \times 10^5$	u', v'
Lawn (1971)	$3.8 \times 10^4 \sim 2.5 \times 10^5$	u', v'
Townes *et al.* (1972)	$3.0 \times 10^4 \sim 4.8 \times 10^5$	u', v'
Perry & Abell (1975)	$7.8 \times 10^4 \sim 2.6 \times 10^5$	u', v'
Perry, Henbest & Chong (1986)	$7.5 \times 10^4 \sim 2.0 \times 10^5$	u', v'
Morrison *et al.* (2004)	$5.5 \times 10^4 \sim 5.7 \times 10^6$	u'

TABLE 1. Existing turbulence data in fully developed pipe flow.

high-Reynolds-number turbulence. Here, we present measurements of the wall-normal component of turbulence in fully developed pipe flow for $1.1 \times 10^5 \leqslant Re_D \leqslant 6.2 \times 10^6$ to complement the work by Morrison *et al.* (2004), and to provide additional insight on high-Reynolds-number turbulence. Previous measurements of this component were for Reynolds numbers less than 5×10^5 (see table 1), and so the present data extend the data base by more than an order of magnitude, and reveal new aspects of the scaling behaviour.

2. Turbulence scaling

Townsend (1976) proposed that near-wall turbulence is a combination of locally active motions (u_i) and inactive motions (u_o). Here, $\overline{u_i^2}$ is the inner-flow-induced or active motion that scales on inner-layer parameters (velocity scale u_τ and length scale ν/u_τ), and $\overline{u_o^2}$ is the outer-flow-induced or inactive motion that scales on outer-layer parameters (velocity scale u_τ and length scale δ or R). As usual, $u_\tau = \sqrt{\tau_w/\rho}$, where τ_w is the wall shear stress and ρ is the fluid density. The active motions are those that are expected to contribute to the shear stress $-u'v'$, whereas the inactive motions are seen as large eddies 'meandering or swirling' in the near-wall region that contribute only to the wall-parallel components u' and w'. Based on Townsend's arguments, there is no strong interaction between inactive and active motions when the Reynolds number is sufficiently high, so the streamwise turbulence intensity is just a linear superposition of the two. That is, $\overline{u'^2} = \overline{u_i^2} + \overline{u_o^2}$. However, the peak values of $\overline{u'^2}$ and $\overline{w'^2}$ in the near-wall region do not collapse with inner-layer parameters, but increase indefinitely with Reynolds number (see, for example, Metzger *et al.* 2001), indicating the continuing influence of the inactive motions in the near-wall region. For the wall-normal component in the inner region, Townsend's hypothesis predicts that $v' \sim v_i$, and $\overline{v'^2}^+ = f(y^+)$, where $y^+ = yu_\tau/\nu$. One of the aims of the present study is to obtain high-quality data on v' at high Reynolds numbers to verify these expectations.

A more detailed physical model based on Townsend's hypothesis, called the 'attached eddy model', was developed by Perry & Chong (1982), Perry *et al.* (1986), Perry & Marusic (1995) and Marusic & Perry (1995). Here, near-wall turbulence is modelled as the linear superposition of a number of hierarchies of self-similar attached eddies, with the number of hierarchies increasing with Reynolds number. By using dimensional analysis and overlap arguments, two self-similar regions in the spectra were proposed for the streamwise component of turbulence: one that follows a k^{-1} law and another that follows a $k^{-5/3}$ law. The $k^{-5/3}$ scaling is expected to be universal for high wavenumbers, but the k^{-1} scaling is expected to appear only for wall distances that lie within the overlap region for the mean flow (in our case, where $600 < y^+ < 0.12R^+$). At sufficiently high Reynolds numbers, the k^{-1} behaviour should

appear using both inner and outer scaling in order to be self-similar. That is,

$$\frac{\phi_{11}(k_1 y)}{{u_\tau}^2} = \frac{A_1}{k_1 y}, \tag{2.1}$$

$$\frac{\phi_{11}(k_1 R)}{{u_\tau}^2} = \frac{A_1}{k_1 R}, \tag{2.2}$$

where $\phi_{11}(k_1 y)$ is the energy density per unit non-dimensional wavenumber $k_1 y$, k_1 is the streamwise wavenumber, and A_1 is a universal constant which depends on the particular eddy shape adopted in the model. The presence of this scaling denotes that complete similarity is achieved (that is, it is independent of Reynolds number).

A similar analysis was proposed for the wall-normal component. Because eddies of scale R are damped first by the wall (the impermeability constraint), asymptotic matching with inner and outer scales is not possible, and only one self-similar region is found, that is, a region of $k^{-5/3}$ scaling. The k^{-1} scaling is not expected to appear in the ϕ_{22} spectra.

Broadband turbulence intensity distributions are obtained from these spectral arguments by integrating over the various spectral regions (Perry *et al.* 1986). Hence:

$$\frac{\overline{u'^2}}{{u_\tau}^2} = B_1 - A_1 \ln\left(\frac{y}{R}\right) - C_1 (y^+)^{-1/2}, \tag{2.3}$$

$$\frac{\overline{v'^2}}{{u_\tau}^2} = B_3 - \frac{4}{3} C_1 (y^+)^{-1/2}, \tag{2.4}$$

where C_1 is another universal constant, and B_1 and B_3 are characteristic constants that vary with the flow geometry (boundary layer, pipe, or channel). The pipe flow measurements by Perry *et al.* (1986) over a Reynolds number range of 7.5×10^4 to 2.0×10^5 supported the proposed model, and Perry & Li (1990) and Marusic *et al.* (1997) extended the model to zero-pressure gradient turbulent boundary layers for arbitrarily high Reynolds numbers.

Recently, Morrison *et al.* (2004) presented measurements of the streamwise velocity fluctuations in pipe flow for Reynolds numbers from 5.5×10^4 to 5.7×10^6. Turbulence intensities, moments up to sixth order, and frequency spectra were obtained.

The $\overline{u'^2}$ distributions displayed two maxima. The first maximum was located near $y^+ = 15$, the point where the production of turbulence kinetic energy also reaches its maximum. Its peak value increased with Reynolds number, as seen by Fernholz & Finley (1996) and Metzger *et al.* (2001). Morrison *et al.* (2004) proposed that the inactive motion 'is somewhat of a misnomer' because the outer-layer motions clearly contribute to the energy in the near-wall region by producing shear even at very high Reynolds numbers. The second maximum, at $y^+ \approx 500$, appears only for $Re_D > 2 \times 10^5$, and increases indefinitely with Reynolds number, as does its distance from the wall, suggesting a continued influence of viscosity in the outer region even at very high Reynolds numbers.

In contrast to the conclusions drawn by Perry and co-workers, Morrison *et al.* found that the spectra did not show complete similarity even for Reynolds numbers up to 5.5×10^6. At the highest Reynolds number a limited collapse of the spectra at different wall distances was found in the region of $k_1 y \sim 1$, but there was no clear region that displayed a ${k_1}^{-1}$ slope. In addition, this wavenumber region in inner scaling did not collapse in outer scaling, and vice versa. In other words, complete similarity was not shown at any Reynolds number up to 5.5×10^6. The probability density functions were also tested for similarity, and similarly no collapse was found for either different

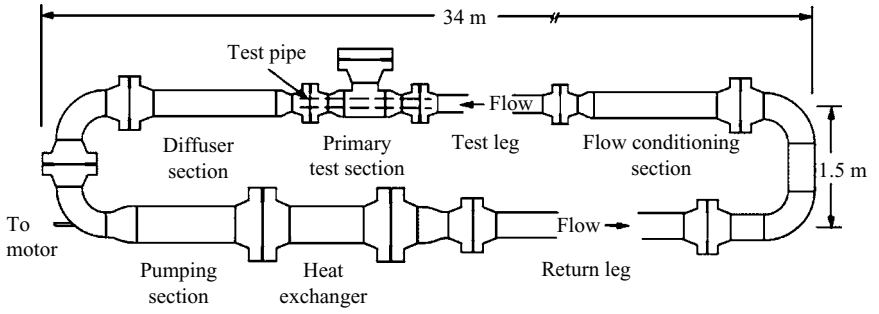

FIGURE 1. Princeton/DARPA-ONR Superpipe facility.

y^+ locations at the same Reynolds number, or for different Reynolds numbers at the same y^+ location.

Recently, Nickels *et al.* (2005), in a study of a boundary layer at $Re_\theta = 3.45 \times 10^4$, observed a $k_1{}^{-1}$ region covering about 1/3 of a decade very close to the wall at $y/\delta = 0.007$. They estimated that one decade of $k_1{}^{-1}$ behaviour would be seen at $y/\delta = 0.0019$ for $Re_\theta = 1.38 \times 10^5$ (equivalent to $Re_D \approx 2.76 \times 10^6$), and that no $k_1{}^{-1}$ behaviour can exist for $y/\delta > 0.019$. Thus the $k_1{}^{-1}$ scaling, if it exists at all, is expected to be confined to a very small region of the flow, even at high Reynolds number.

These observations on self-similarity lead to a new evaluation for the similarity argument itself and the inactive motion concept. The present study extends the work of Morrison *et al.* (2004) on the streamwise component to an evaluation of the wall-normal component of turbulence, a crucial feature of the active motions.

3. Experimental methods

All data presented in this paper were acquired using hot-wire anemometry in the Princeton/DARPA-ONR Superpipe Facility (see figure 1). The facility uses compressed air at pressures up to 200 atm as the working fluid, and produces fully developed turbulent pipe flow at Reynolds numbers from 3.1×10^4 to 3.5×10^7. The test pipe has an internal diameter of $D = 129.36 \pm 0.08$ mm. The surface finish of the test pipe is estimated as 0.15 ± 0.03 μm, and the surface is smooth for all 2.1×10^7, which is greater than all Reynolds numbers studied here (see McKeon *et al.* 2004 and Shockling, Allen & Smits 2006). The first access port (the location used for all turbulence measurements) is located $160D$ downstream of the entrance. A fixed Pitot tube recorded the centreline velocity U_{cl} at the second access port located about $35D$ downstream from the first. The pressure gradient was measured using twenty static wall pressure taps placed between the first and second ports over a distance of $25D$. Further details on the facility and the measurement techniques used here are given by Zagarola & Smits (1998), Zagarola (1996), McKeon *et al.* (2004) and Zhao (2005).

Crossed hot-wire probes were used to measure the streamwise and wall-normal components of turbulence. The probes were made at the University of Poitiers in France and used tungsten wires with diameters of 2.5 μm and lengths of $l \approx 0.5$ mm. The distance between the two wires was approximately 0.5 mm. To facilitate measurements close to the wall, the hot-wire probe was inclined towards the wall at about 7° from the mean flow direction.

The wires were operated in constant temperature mode using the Dantec Streamline system. A Krohn-Hite-3382 filter was used to low-pass the signals at $f_c = 0.1$ Hz to obtain the DC component, and a Krohn-Hite-3988 filter was used to band-pass the

Re_D	y_0^+	l^+
1.1×10^5	30	20
1.4×10^5	50	28
4.8×10^5	155	76
1.1×10^6	322	164
9.8×10^6	2494	1226

TABLE 2. Non-dimensional wire length l^+, and non-dimensional wall distance of the first point y_0^+ at different Reynolds numbers.

fluctuating component ($f_c \leqslant f \leqslant f_s/2$). The low-pass signal was sampled at 1 kHz, and the high-pass signals were sampled at $f_s = 50$ kHz (except for experiments with $Re = 9.8 \times 10^6$ where f_s was 75 kHz). At each location in the profile, 90×10^6 data points were obtained, corresponding to 1800 s in real time (except for $Re = 9.8 \times 10^6$ where it corresponds to 1400 s). The signals were digitized and analysed using National Instruments boards and Labview software.

The probes were calibrated using a new method developed by Zhao *et al.* (2004) called 'stress calibration', which uses the fact that the total stress in a fully developed turbulence pipe is known from the streamwise pressure drop. Stress calibration was demonstrated to be more accurate than the traditional angle calibration method or the dynamic procedure suggested by Perry (1982) (see Zhao & Smits 2006).

Because of geometrical limitations, y_0, the closest distance to the wall at which the crossed wires could be placed, was 1.40 mm. Table 2 shows y_0^+ at each Reynolds number studied. It is clear that the flow in the near-wall region is inaccessible to the crossed-wire probe even at the lowest Reynolds number. This is an important limitation on the measurements, but our main focus is on the overlap region (the log-law region in the mean velocity profiles, that is, the region $y^+ \geqslant 500$ and $y/R \leqslant 0.1$). Note that $y_0/R = 0.02$.

The spatial resolution of the probe is normally presented in terms of the non-dimensional wire length $l^+ = lu_\tau/\nu$, which varies with Reynolds number as shown in table 2. It is usually assumed that all the scales of turbulence will be resolved for $l^+ \leqslant 10$ (see, for example, Klewicki & Falco 1990). According to Khoo, Chew & Li (1997), however, measurements with $l^+ \leqslant 22$ will be fully resolved for $y^+ \geqslant 5$, and according to this criterion the spatial resolution of the measurements at $Re_D = 1.1 \times 10^5$ and 1.4×10^5 are probably adequate, since the minimum wall distances are $y_0^+ = 30$ and 50, respectively. The measurements at higher Reynolds numbers, however, are affected to a greater or lesser degree by the limited spatial resolution of the probe.

To estimate the effects on the spectra and the broadband turbulence intensity, we use the work of Wyngaard (1968). According to Wyngaard, if it is assumed that the high-wavenumber region follows a universal scaling based on the Kolmogorov length scale $\eta = (\nu^3/\epsilon)^{1/4}$, where the dissipation rate ϵ is estimated as $\epsilon = 15\nu \int k^2 \phi(k)\, \mathrm{d}k$, then a wavenumber can then be found for a given attenuation percentage in the energy at that wavenumber. The wavenumbers for a 10 % attenuation (k_{10}) are given in table 3.

The estimated errors on the broadband turbulence intensities are shown in table 4. Figure 2 illustrates how these estimates were obtained for a specific case ($Re = 1.1 \times 10^5$ and $y/R = 0.1$). The spectrum in the high-wavenumber portion is replaced by $k^{-5/3}$ law that blends into Wyngaard's form of the dissipation spectrum, based on a known or estimated value of the Kolmogorov length scale. It was not

	l/η			$k_{10}(\mathrm{m}^{-1})$		
Re_D	$y/R=0.05$	0.1	1	0.05	0.1	1
1.4×10^5	8	7	4	2200	2400	3000
4.8×10^5	20	17	10	1400	1400	1600
1.1×10^6	44	38	21	1200	1200	1400
9.8×10^6	236	200	100	1000	1000	1100

TABLE 3. Wire length in terms of the Kolmogorov length scale, and cutoff wavenumber k_{10} where a 10 % attenuation in the spectrum is expected.

	$\overline{u^2}$			$\overline{v^2}$		
Re_D	$y/R=0.05$	0.1	1.0	0.05	0.1	1.0
4.8×10^5	1	1	1	3	3	2
1.1×10^6	1.4	1.2	1.1	4	4	3

TABLE 4. Percentage error estimates on attenuation of small-scale motions due to spatial filtering.

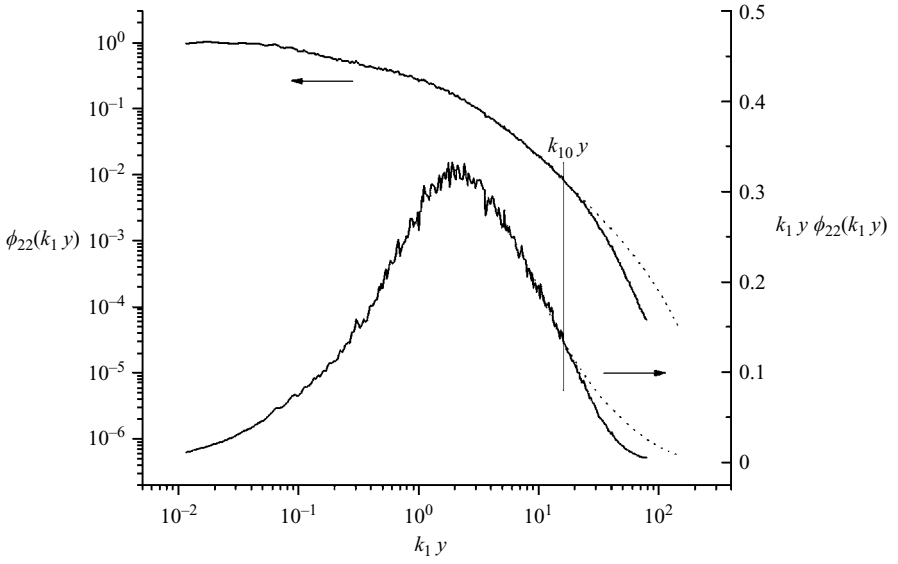

FIGURE 2. Procedure for estimating the errors in the turbulence intensities (for $Re=1.1\times10^5$ and $y/R=0.1$) due to limited spatial resolution. ——, measured spectrum; - - -, extrapolated spectrum based on Wyngaard (1968)'s analysis.

possible to make this estimate at $Re_D=9.8\times10^6$ because the spectra in the high-wavenumber region are contaminated by additional effects.

Temporal resolution is also an issue. To fully resolve the turbulence in time, the frequency response of the instrument needs to be higher than Kolmogorov frequency, which increases with Reynolds number, that is, $f_K\sim U\sqrt{Re_D}/D$. In our experiments,

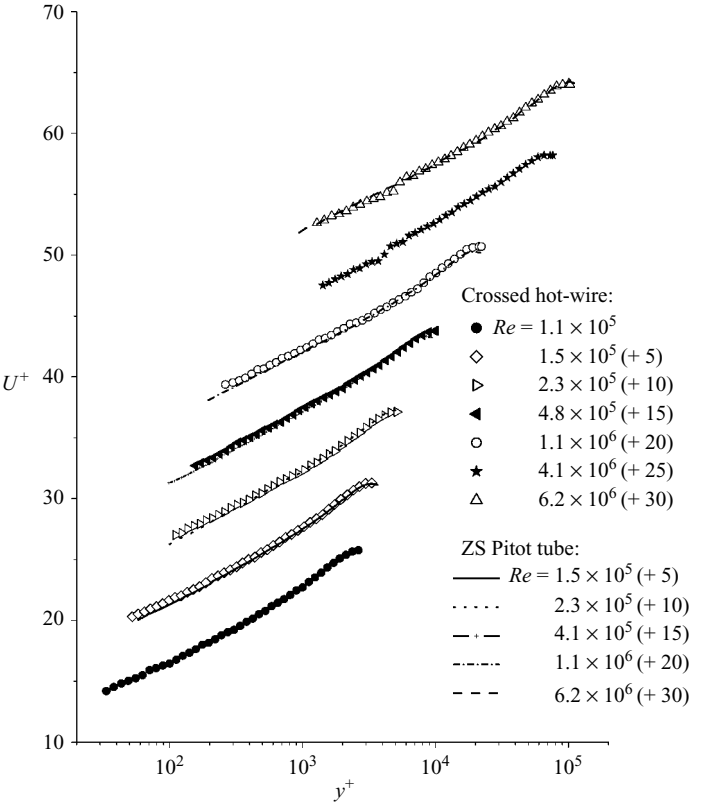

FIGURE 3. Mean velocity measurement for Reynolds number from 1.1×10^5 to 6.2×10^6. Zagarola & Smits (1998) Pitot tube data shown are corrected by McKeon *et al.* (2003). Successive velocity profiles are offset by $\Delta U^+ = 5$ for clarity.

f_K ranges from about 24 kHz at $Re_D \sim 10^5$, to about 244 kHz at $Re_D \sim 10^7$. The frequency response of the hot-wire anemometry system was in the range of 60 kHz $\sim$ 100 kHz, so that at the highest Reynolds number the dissipation range is not fully resolved for lack of frequency response (independent of any spatial filtering that may also be present).

One final source of error in the crossed hot-wire measurements is the so-called binormal cooling effect, which is the additional heat transfer due to the velocity component normal to the hot-wire measurement plane (w' in current study). According to Zhao & Smits (2006), neglecting this additional heat transfer can lead to significant errors, but for the present measurements the errors are generally small. For example, in the near-wall region where turbulence level is high, at $Re = 1.4 \times 10^5$, the errors are about 1.5 %, 3 %, 0.5 % and 1 % for $\overline{U}$, $\overline{u'v'}$, $\overline{u'^2}$ and $\overline{v'^2}$ respectively.

4. Experimental results

To verify that the crossed-wire probe was performing satisfactorily, the mean velocity and streamwise turbulence intensity results were compared with previous data obtained in the same facility. The mean velocity profiles for Reynolds numbers from 1.1×10^5 to 6.2×10^6 are shown in figure 3, scaled using inner variables so that $U^+ = U/u_\tau$ and $y^+ = yu_\tau/\nu$. The results are compared with the Pitot tube

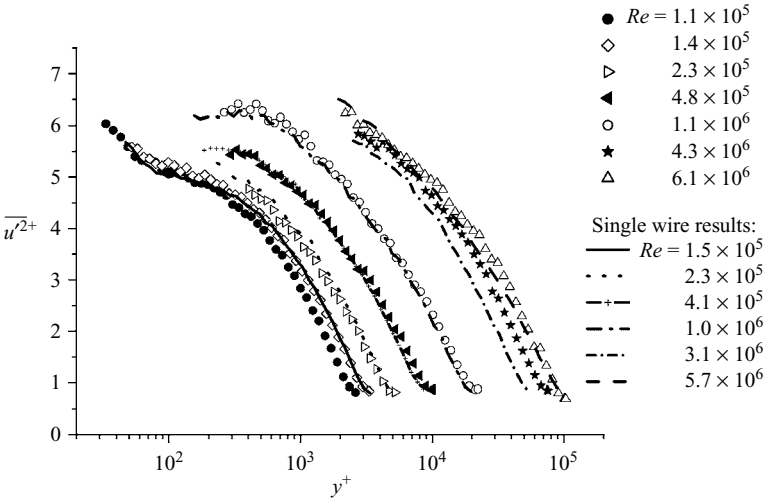

FIGURE 4. The streamwise turbulence intensity $\overline{u'^2}$ inner scaling. Single-wire results are from Morrison *et al.* (2004).

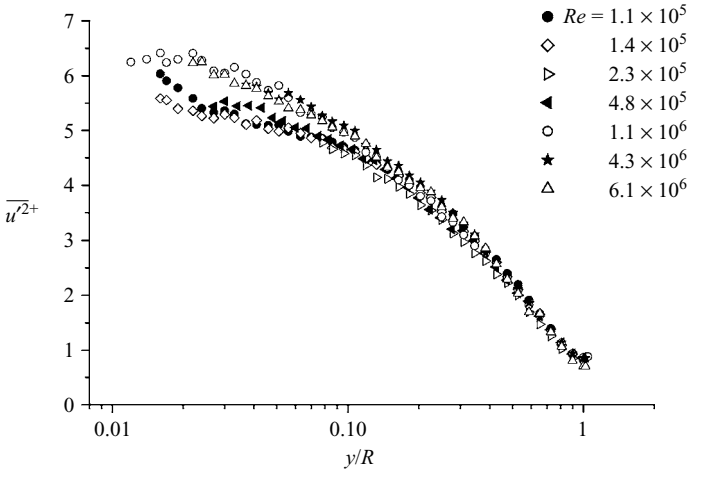

FIGURE 5. The streamwise turbulence intensity $\overline{u'^2}$ in outer scaling.

measurements obtained by Zagarola & Smits (1998), as corrected by McKeon *et al.* (2004). Good agreement is found except in the near-wall region, where the crossed hot-wire data are slightly higher than the Pitot tube data. This trend is consistent in sense and magnitude with the effects of binormal cooling as described by Zhao & Smits (2006).

The streamwise turbulence data are shown in figure 4 in inner-layer coordinates, where $\overline{u'^2}^+ = \overline{u'^2}/u_\tau{}^2$. Generally, the crossed hot-wire data agree very well with the single-wire data obtained by Morrison *et al.* (2004). The near-wall peak near $y^+ = 15$ is not shown in the present measurements because the crossed hot-wire cannot access this region. Figure 5 shows the crossed-wire data in outer-layer coordinates. A collapse was found for $y/R \geqslant 0.4$, but as found by Morrison *et al.* there is no collapse in the

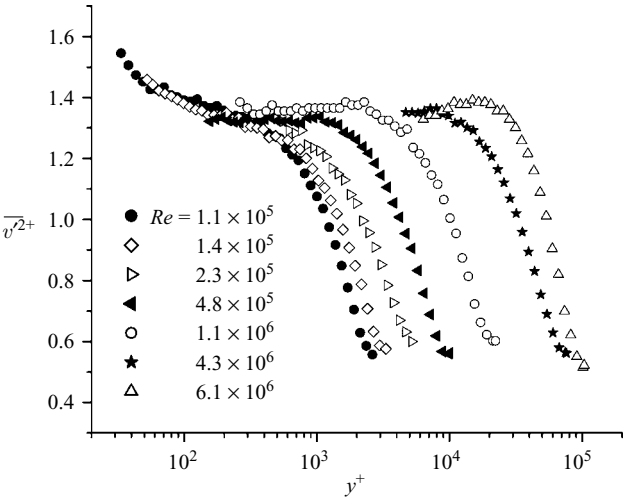

FIGURE 6. The wall-normal turbulence intensity $\overline{v'^2}^+$ in inner scaling.

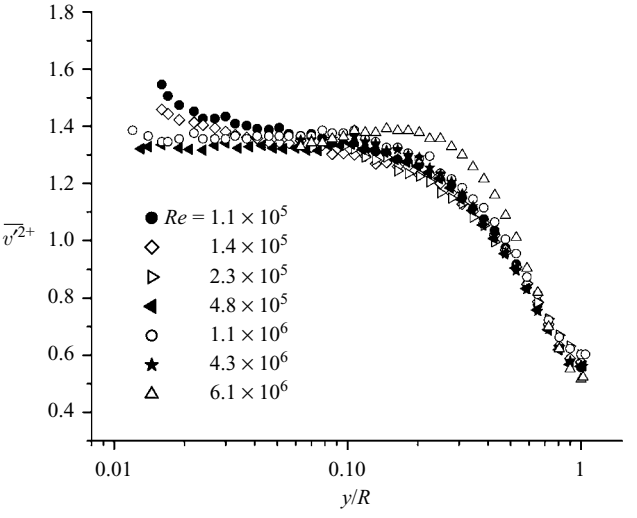

FIGURE 7. The wall-normal turbulence intensity $\overline{v'^2}^+$ in outer scaling.

overlap region ($600 \leqslant y^+ \leqslant 0.12R^+$). Although this observation suggests a Reynolds number dependence, the effects of spatial filtering prevent a more definite conclusion.

The wall-normal component v' data are shown in inner and outer scaling in figures 6 and 7, respectively. In inner scaling the data demonstrate a collapse in the overlap region for Reynolds numbers higher than 4.8×10^5, and the value for v'^+_{rms} in this region is constant around 1.15. Somewhat unexpectedly, however, the wall-normal intensity levels rise for $y^+ \leqslant 50$. This trend is obvious only for the two lowest Reynolds numbers, but the presence of a near-wall peak in the wall-normal turbulence intensity is suggested. The near-wall peak in the streamwise turbulence intensity is well known, and its increase with Reynolds number is attributed to the influence of inactive motion originally proposed by Townsend (1976). The presence of a similar peak in the wall-normal component behaviour may provide further evidence for the

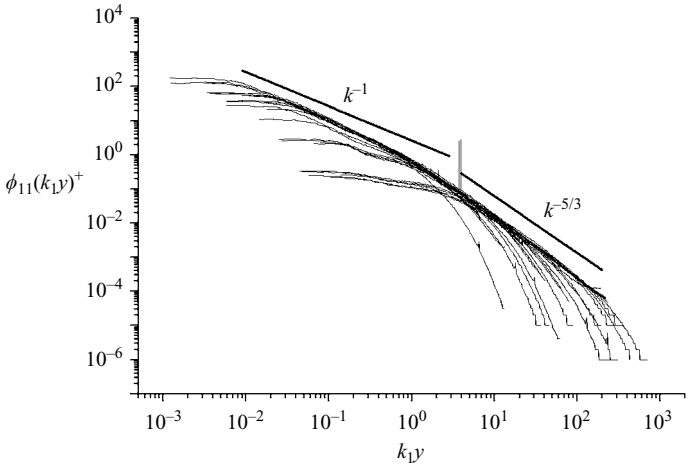

FIGURE 8. Spectra of the streamwise component for all Reynolds numbers from 1.1×10^5 to 9.8×10^6.

nonlinear interaction between locally active motion and the outer inactive motions. Unfortunately, the present results can only hint at the behaviour of this peak, and further measurements with better spatial resolution will be needed to investigate it more fully.

The data for $\overline{v'^2}$ in outer scaling (figure 7) also demonstrate a reasonable collapse in the overlap region, independent of Reynolds number. At first sight, the collapse seems to support the attached eddy model, in the sense that the inner and outer flow influences appear to be small in the overlap region. We shall see that this conclusion is not supported by the wall-normal spectra presented below. In the outer region, collapse is also found for $y/R \geqslant 0.4$, as in the streamwise intensity outer scaling result, except for the highest Reynolds number where the data seem unreasonably high compared to the other profiles. It is not clear what would cause this deviation to occur. It is true that at higher Reynolds numbers the air density is high, and the hot-wire requires a high current level to maintain a given overheat ratio. Since there are limits on the maximum current available, the overheat ratio at higher Reynolds numbers needs to be reduced, which reduces its sensitivity. In addition, the high current levels may lead to nonlinearities in the instrument response. Furthermore, the high mass flow rate at high Reynolds number places an extra load on the wire, which may bend in response. There is no evidence that the calibration was affected (indeed, the correlation coefficient was 0.998 or better for all Reynolds numbers), but the effective angle of the wires changed a few degrees with Reynolds number. Although it is not obvious why any of these effects would cause a systematically high value for $\overline{v'^2}$ at the highest Reynolds number, these considerations suggest that some caution should be exercised in interpreting the data at 6.1×10^6.

Figures 8 and 9 show the streamwise turbulence spectra scaled using inner variables for Reynolds numbers from 1.1×10^5 to 9.8×10^6. The streamwise wavenumber k_1 is deduced using Taylor's hypothesis, so that $k_1 = 2\pi f/U$. We should note that similar data were obtained by Morrison *et al.* (2004) using single wires, but their low-wavenumber results were under-resolved because they used relatively short record lengths. Later analysis by McKeon and Morrison (private communication) using longer record lengths yielded results that agree very well with the data presented here.

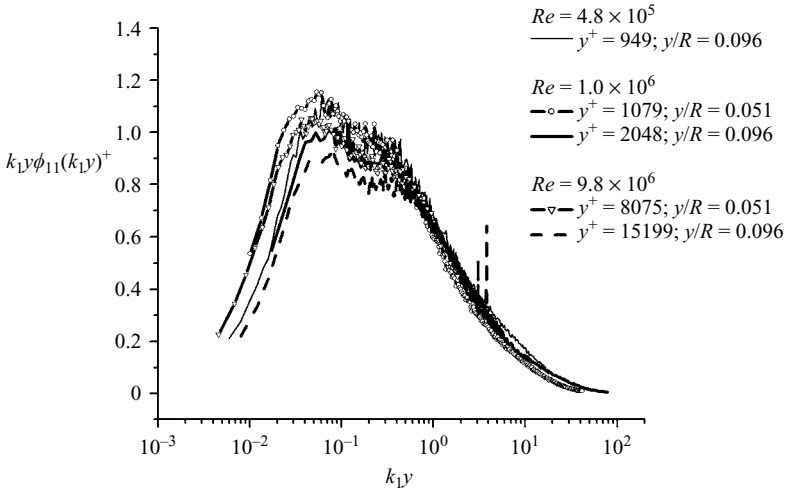

FIGURE 9. Spectra of the streamwise component in the overlap region in pre-multiplied form for selected Reynolds numbers.

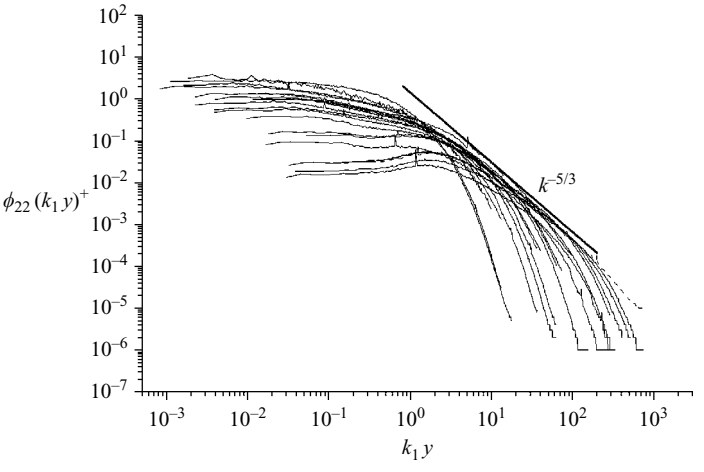

FIGURE 10. Spectra of the wall-normal component at all Reynolds numbers.

Particular attention was given to spectra in the overlap region. The data collapse only in a limited region around $k_1 y \sim 1$ where the spectra cross. According to the attached eddy model (Perry *et al.* 1986; Perry & Marusic 1995; Marusic & Perry 1995), a collapse showing a k^{-1} behaviour (that is, a flat region in the pre-multiplied spectra) is expected, with the level corresponding to a universal constant A_1. In the results obtained here (figure 9), there is no collapse to a k^{-1} behaviour, and no universal constants are found. This result agrees with Morrison *et al.* (2004), who also found no similarity behaviour in the overlap region.

The spectra for the wall-normal component are shown in figure 10 for Reynolds numbers from 1.1×10^5 to 9.8×10^6. No k^{-1} region is found, although a reasonably extensive $k^{-5/3}$ region is apparent.

Some selected spectra in the overlap region are shown in figures 11–13. In inner scaling (figure 11), good collapse is found for all spectra for $1 \leqslant k_1 y \leqslant 10$, and for

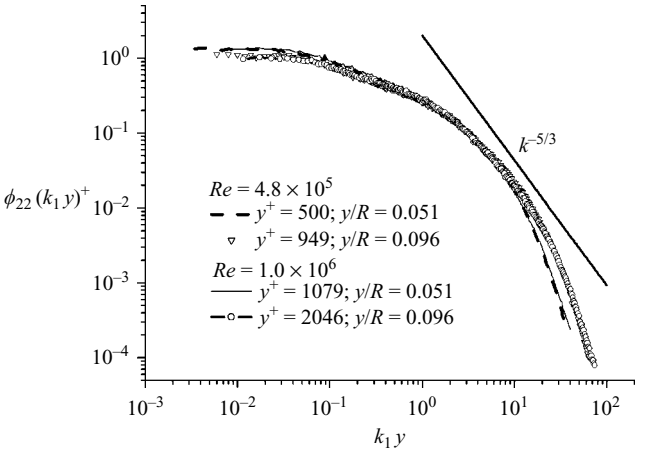

FIGURE 11. Spectra of the wall-normal component in the overlap region using inner scaling.

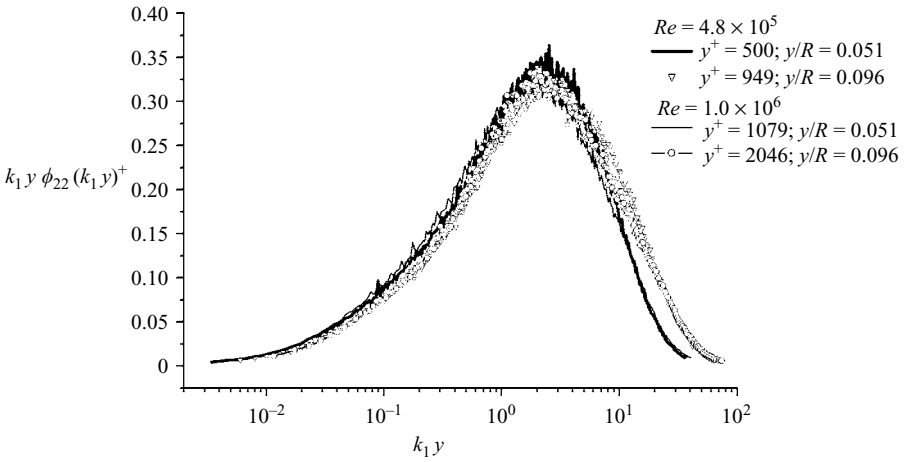

FIGURE 12. Spectra of the wall-normal component in the overlap region using inner scaling in pre-multiplied form.

those spectra with the same y/R, good collapse is also found for $k_1y \leqslant 1$. It appears, therefore, that the outer flow (that scales on u_τ and R) affects the wall-normal motion in the overlap region, so that the similarity behaviour expected from the attached eddy model does not occur, at least for Reynolds numbers up to 10^6. Figure 12 shows the same data in pre-multiplied form. The most energy-containing eddies lie in the region $1 \leqslant k_1y \leqslant 10$, and significant energy is contained in very low wavenumbers: about one-third of the total energy in the wall-normal component is contained in $k_1y \leqslant 1$. Note that the streamwise spectra (figure 9) peaks around $k_1y \approx 0.1$ at the same wall distance, so that the energy-containing scales of u' are much longer than those of v'.

In outer scaling (figure 13), no general collapse is found in any wavenumber region, but for spectra at the same radial position a collapse is found for $k_1R \leqslant 20$ and $k_1R \geqslant 200$.

The shear stress spectra (cospectra) in the overlap region are shown in figures 14–17. According to the attached eddy model, the major contribution to the Reynolds

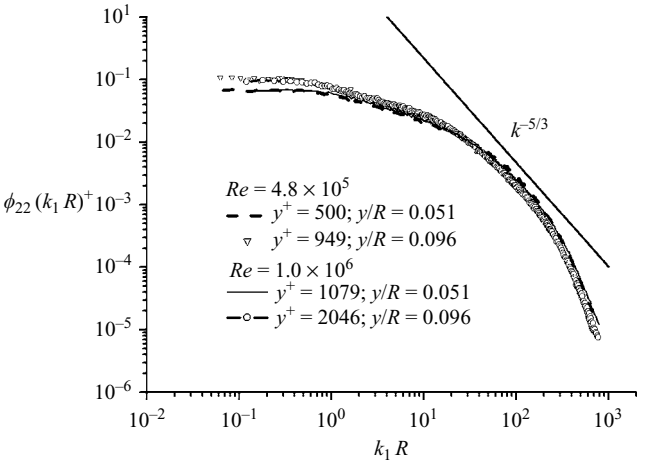

FIGURE 13. Spectra of the wall-normal component in the overlap region using outer scaling.

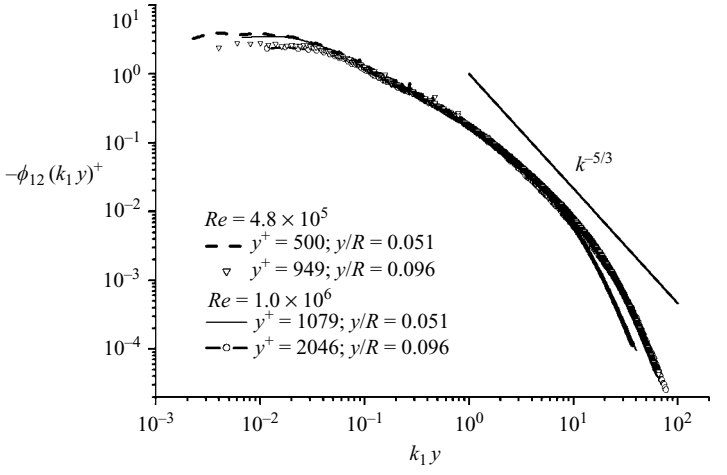

FIGURE 14. Cospectra of $u'v'$ in the overlap region using inner scaling.

shear stress comes from local eddies, so the spectra are expected to collapse for the entire inner-scaled wave-number region. In our results (figure 14), a good collapse was found for the region of $0.1 \leqslant k_1 y \leqslant 10$, but in the low-wavenumber region collapse was only found for spectra at the same y/R locations, indicating an influence from the outer flow. The pre-multiplied spectra (figure 15) highlight the collapse found for the energy-containing wavenumbers ($k_1 y \sim 1$). In outer-layer coordinates (figures 16 and 17), there is no obvious similarity behaviour evident.

5. Discussion and conclusions

For the streamwise turbulence intensity, as reported earlier by Morrison *et al.* (2004), it was found that the data do not collapse with inner scaling, but with outer scaling a collapse within $\pm 10\,\%$ is found for $y/R \geqslant 0.4$. The streamwise turbulence spectra within the overlap region for the mean flow ($600 \leqslant y^+ \leqslant 0.12R^+$) were used to search for similarity behaviour, especially the k^{-1} law. Using inner scaling, collapse

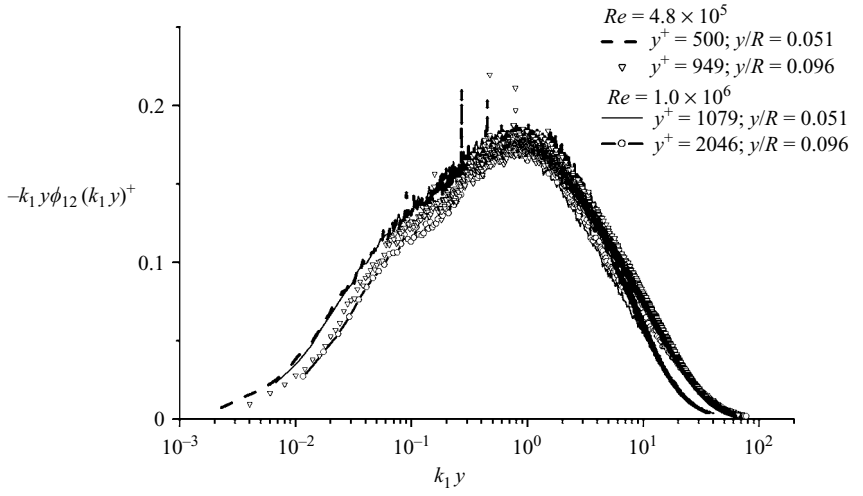

FIGURE 15. Cospectra of $u'v'$ in the overlap region using inner scaling in pre-multiplied form.

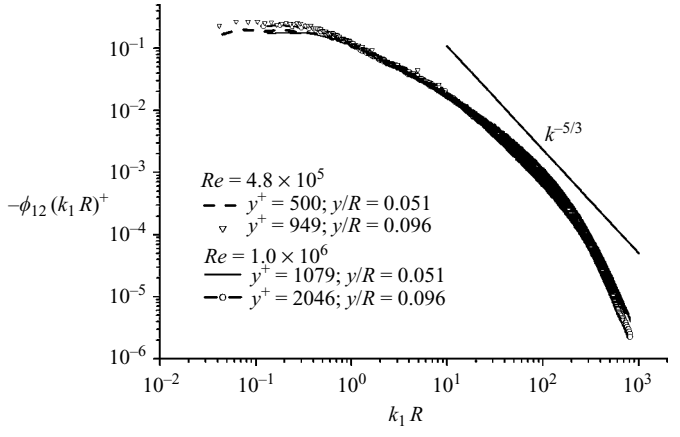

FIGURE 16. Cospectra of $u'v'$ in the overlap region using outer scaling.

was found only for a limited region around $k_1 y \sim 1$ where the spectra cross each other, but no prominent k^{-1} region was found. As proposed by Perry *et al.* (1986), Perry & Marusic (1995) and Marusic & Perry (1995), k^{-1} scaling is expected in the shoulder (flat) region, and the level corresponds to a universal constant A_1. However, the results reported here still show a Reynolds number dependence and a y/R dependence in the wavenumber region of $k_1\nu/u_\tau \ll k_1 y \ll k_1 R$. This result could reflect the incomplete similarity proposed by Morrison *et al.* (2004), which suggests that outer-flow-inactive motions interact with the near-wall motions in a nonlinear way. This seems to be the most likely explanation, as based on the wall-normal turbulence measurements results obtained here and by Morrison *et al.* Alternatively, y/R may not be small enough to see a prominent k^{-1} region. According to Nickels *et al.* (2005), y/R may need to be less than about 0.01 to observe a prominent ${k_1}^{-1}$ region at these Reynolds numbers.

It is instructive to compare the high-Reynolds-number pipe flow spectra with boundary-layer data at comparable Reynolds numbers. The atmospheric layer

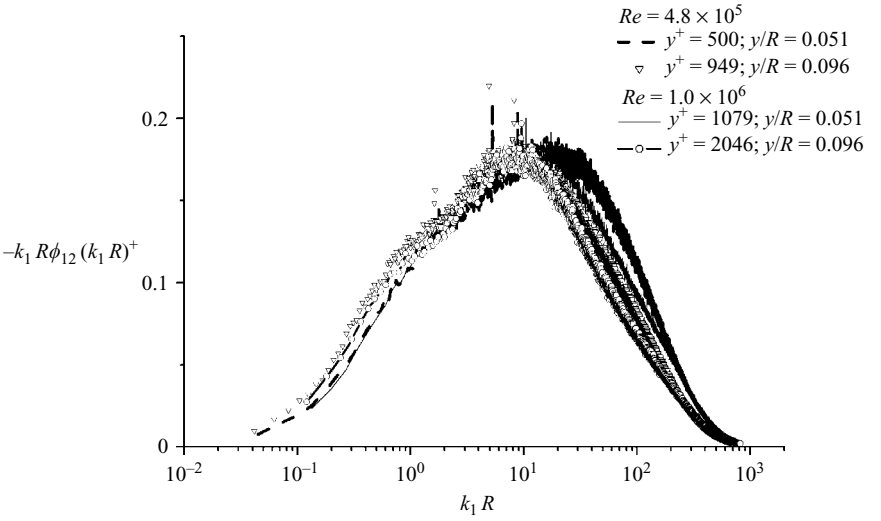

FIGURE 17. Cospectra of $u'v'$ in the overlap region using outer scaling in pre-multiplied form.

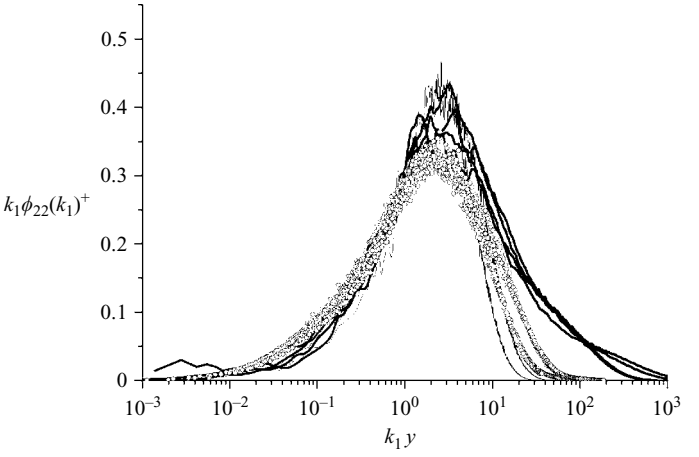

FIGURE 18. Wall-normal spectra in pipe flow and boundary layer flows. ——, atmospheric data, $Re_\tau = 3 \times 10^6$ (Marusic *et al.* 2001); ——, laboratory data, $Re_\tau = 3.5 \times 10^3$ (Marusic *et al.* 2004); ○, Superpipe data $Re_D = 4.8 \times 10^5$ ($Re_\tau = 2 \times 10^4$); $Re_D = 1.1 \times 10^6$ ($Re_\tau = 4.2 \times 10^4$).

typically has $Re_\theta \approx 10^6$ (Marusic, Kunkel & Porte-Agel 2001), which has an equivalent $Re_D \approx 2 \times 10^7$. Figures 18 and 19 show this comparison. The wall-normal and cospectra from the pipe experiment fall below the boundary layer spectra. For the energy-containing part, the pipe spectra are very close to the atmospheric spectra, given that atmospheric data are not as well converged as the Superpipe data.

For the wall-normal turbulence intensities, a collapse for $y^+ \geqslant 200$ and $y/R \leqslant 0.1$ was found for Reynolds numbers from 1.1×10^5 to 1.0×10^6. The collapse corresponds to a region of constant ($v'_{\text{r.m.s.}}$) around $1.15u_\tau$. The wall-normal turbulence intensity appeared to also show the start of a maximum near the wall (figure 6). This rise looks similar to the first maximum found in the streamwise turbulence intensity profile at about $y^+ \sim 15$, and may show an influence of the outer flow on the wall-normal components in the near-wall region. This observation cannot be explained using

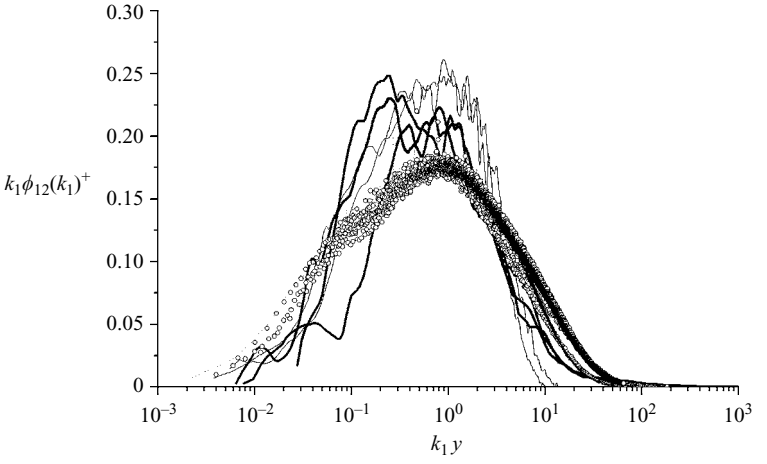

FIGURE 19. Cospectra in pipe flow and boundary layer flows. Symbols as in figure 18.

Townsend's inactive motion concept, but is in accord with Morrison *et al.*'s incomplete similarity arguments: the near-wall motion ($y^+ \sim 15$) is influenced by the outer flow, and due to the intrinsic nonlinearity of the Navier–Stokes equation, so there is no clear-cut distinction between active and inactive motions and no complete similarity exists. Further measurements in the near-wall region at high Reynolds numbers are urgently needed, but they are technically challenging because of the experimental limitations that occur, as amply demonstrated in the current contribution.

The spectra of the wall-normal component and cospectra were consistent with the behaviour of the wall-normal and streamwise intensities. Similarity was found when using inner-scaling parameters, but the influence of the outer flow persisted in the low-wavenumber regions for near-wall region ($y/R \geqslant 0.051$) and Reynolds numbers up to 1.0×10^6. Again, a nonlinear interaction between inner flow and outer flow in the near-wall region is suggested.

The support of ONR under Grant No. N00014-03-1-0320 and NSF Grant CTS-0306691 is gratefully acknowledged. We also wish to thank Jonathan Morrison for many useful discussions and James Allen and the University of Poitiers for providing the hot-wire probes.

REFERENCES

DEGRAAFF, D. B. & EATON, J. 2000 Reynolds-number scaling of the flat-plate turbulent boundary layer. *J. Fluid Mech.* **422**, 319–346.

FERNHOLZ, H. H. & FINLEY, P. J. 1996. Incompressible zero-pressure-gradient turbulent boundary layers: An assessment of the data. *Prog. Aerospace Sci.* **32**, 245–311.

FERNHOLZ, H. H., KRAUSE, E., NOCKEMANN, N. & SCHOBER, M. 1995. Comparative measurements in the canonical boundary layer at $Re_{\delta_2} \leqslant 6 \times 10^4$ on the wall of the German–Dutch windtunnel. *Phys. Fluids* **7**, 1275–1281.

KHOO, B. C., CHEW, Y. T. & LI, G. L. 1997 Effects of imperfect spatial resolution on turbulence measurements in the very near-wall viscous sublayer region. *Exps. Fluids* **22**, 327–335.

KLEWICKI, J. C. & FALCO, R. E. 1990 On accurately measuring statistics associated with small-scale structure in turbulent boundary layers using hot-wire probes. *J. Fluid Mech.* **219**, 119–142.

KUNKEL, G. J. & MARUSIC, I. 2005 Study of the near-wall-turbulent region of the high-Reynolds-number boundary layer using an atmospheric flow. *J. Fluid Mech.* **548**, 375–402.

Laufer, J. 1954 The structure of turbulence in fully developed pipe flow. *NACA Rep.* 1174.

Lawn, C. J. 1971 The determination of the rate of dissipation in turbulent pipe flow. *J. Fluid Mech.* **48**, 477–505.

Marusic, I. & Kunkel, G. J. & Porte-Agel, F. 2001 Experimental study of wall boundary conditions for large-eddy simulation. *J. Fluid Mech.* **446**, 309–320.

Marusic, I., Kunkel, G. J., Zhao, R. & Smits, A. J. 2004 Turbulence intensity similarity formulations for wall-bounded flows. In: *Advances in Turbulence X, Proc. of the 10th European Turb. Conf., CIMNE, Barcelona, Spain* (ed. H. I. Andersson & P.-A. Krogstad).

Marusic, I. & Perry, A. E. 1995 A wall-wake model for the turbulence structure of boundary layers. Part 2. Further experimental support. *J. Fluid Mech.* **298**, 389–407.

Marusic, I., Uddin, A. K. M. & Perry, A. E. 1997 Similarity law for the streamwise turbulence intensity in zero-pressure-gradient turbulent boundary layers, *Phys. Fluids* **9**, 3718–3726.

McKeon, B. J., Ji, J., Jiang, W., Morrison, J. F. & Smits, A. J. 2004 Further observations on the mean velocity distribution in fully developed pipe flow. *J. Fluid Mech.* **501**, 135–147.

McKeon, B. J., Li, J., Jiang, W., Morrison, J. F. & Smits, A. J. 2003 Pitot probe corrections in fully developed turbulent pipe flow. *Meas. Sci. Technol.* **14**, 1449–1458.

McKeon, B. J. & Morrison, J. F. 2005 Inertial scaling and the mixing transition in turbulent pipe flow. *J. Fluid Mech.* (Submitted).

McKeon, B. J. & Smits, A. J. 2003 Static pressure correction in high Reynolds number fully-developed turbulent pipe flow. *Meas. Sci. Technol.* **13**, 1608–1614.

Metzger, M. M., Klewicki, J. C., Bradshaw, K. L. & Sadr, R. 2001. Scaling the near-wall axial turbulent stress in the zero pressure gradient boundary layer. *Phys. Fluids* **13**, 1819–1821.

Morrison, J. F., McKeon, B. J., Jiang, W. & Smits, A. J. 2004 Scaling of the streamwise velocity component in turbulent pipe flow. *J. Fluid Mech.* **508**, 99–131.

Nickels, T. B., Marusic, I., Hafez, S. & Chong, M. S. 2005. Evidence of the k_1^{-1} law in a high Reynolds number turbulent boundary layer. *Phys. Review Lett.* **95**, 074501.

Österlund, J. 1999 Experimental studies of zero pressure-gradient turbulent boundary-layer flow. PhD thesis, Royal Institute of Technology, Stockholm.

Perry, A. E. 1982. *Hot-Wire Anemometry*. Oxford University Press.

Perry, A. E. & Abell, C. J. 1975 Scaling laws for pipe-flow turbulence. *J. Fluid Mech.* **67**, 257–271.

Perry, A. E. & Chong, M. S. 1982 On the mechanism of wall turbulence. *J. Fluid Mech.* **119**, 173–217.

Perry, A. E., Henbest, S. M. & Chong, M. S. 1986 A theoretical and experimental study of wall turbulence. *J. Fluid Mech.* **165**, 163–199.

Perry, A. E. & Li, J. 1990 Experimental support for the attached eddy hypothesis in zero-pressure-gradient turbulent boundary layers. *J. Fluid Mech.* **218**, 405–438.

Perry, A. E. & Marusic, I. 1995 A wall-wake model for the turbulence structure of boundary layers. Part 1. Extension of the attached eddy hypothesis. *J. Fluid Mech.* **298**, 361–388.

Shockling, M. A., Allen, J. J. & Smits, A. J. 2006 Effects of machined surface roughness on high-Reynolds-number turbulent pipe flow. *J. Fluid Mech.* **564**, 267–285.

Townes, H. W., Gow, J. L., Powe, R. E. & Weber, N. 1972 Turbulent flow in smooth and rough pipes. *J. Basic Engin.* **94**, 353–362.

Townsend, A. A. 1976 *The Structure of Turbulent Shear Flow*, 1st edn. Cambridge University Press.

Wyngaard, A. A. 1968 Measurements of small-scale turbulence structure with hot wires. *J. Sci. Instrum.* 2, **1**, 1105–1108.

Zagarola, M. V. 1996 Turbulent pipe flow. PhD thesis, Princeton University, Princeton.

Zagarola, M. V. 1997 Scaling of high-Reynolds number turbulent boundary layers in the National Diagnostic Facility. PhD thesis, Illinois Institute of Technology, Chicago.

Zagarola, M. V. & Smits, A. J. 1998 Mean-flow scaling of turbulent pipe flow. *J. Fluid Mech.* **373**, 33–79.

Zhao, R. 2005 High Reynolds number turbulent pipe flow. PhD thesis, Princeton University, Princeton.

Zhao, R., Li, J. & Smits, A. J. 2004 A new calibration method for crossed hot wires. *Meas. Sci. Technol.* **15**, 1926–1931.

Zhao, R. & Smits, A. J. 2006 Binormal cooling errors on crossed hot-wire measurements. *Exps. Fluids* **40** (2), 212–217.